VLSI silicon multi-gas analyzer coupling gas chromatography and NEMS detectors

J Arcamone, A Niel, V Gouttenoire, M Petitjean, N David, R Barattin, M Matheron, F Ricoul, T Bordy, H Blanc, et al.

VLSI silicon multi-gas analyzer coupling gas chromatography and NEMS detectors

J. Arcamone, A. Niel, V. Gouttenoire, M. Petitjean, N. David, R. Barattin, M. Matheron, F. Ricoul, T. Bordy, H. Blanc, J. Ruellan, D. Mercier, N. Pereira-Rodrigues, G. Costa, V. Agache, S. Hentz, JC Gabriel, F. Baleras, C. Marcoux, T. Ernst, L. Duraffourg, E. Colinet, E.B. Myers*, M.L. Roukes*, P. Andreucci, E. Ollier, and P. Puget

CEA-LETI, MINATEC Campus, 17 rue des Martyrs, F-38054 Grenoble (France)
*Condensed Matter Physics MC 149-33, California Institute of Technology, CA 91125 Pasadena (USA)
Tel: +33 4 38 78 96 95, Fax: +33 4 38 78 24 34, Email: julien.arcamone@cea.fr

ABSTRACT

This work demonstrates for the first time a VLSI-compatible nano/microfabricated, high-performance, portable multi-gas analyzer associating gas chromatography and NEMS resonators.

INTRODUCTION

Designing an integrated gas analyzer providing both high selectivity and high sensitivity to a broad panel of gases still remains a major technological challenge. In the e-nose concept (1), the analyzer architecture is based on a sensor array, each sensor being differently functionalized with a specific layer, each one targeting one single gas in principle. However, it turns out theoretically and experimentally that this concept does not allow estimating the composition of a mixture, even with few analytes (2). Instead, we propose to improve through miniaturization a very classical approach based on the association of a gas-chromatography (GC) column and a detector (Fig.1). The GC provides selectivity by separating in time and space the gas mixture components while detectors sequentially detect the elution peaks at the GC output. In fact, both GC column and detectors can be fabricated with CMOS-compatible VLSI silicon micro- and nanofabrication techniques. As detectors, Nano-Electro-Mechanical Systems (NEMS) resonators were selected for their outstanding mass sensitivity and mass resolution (3). When coating a NEMS with a sensitive layer, a gas adsorption on its surface provokes an increase of the resonator mass which can be estimated through the measurement of a negative resonance frequency shift (4). The system presented hereafter features state-of-the-art experimental results in terms of limit of GC-mediated gas detection.

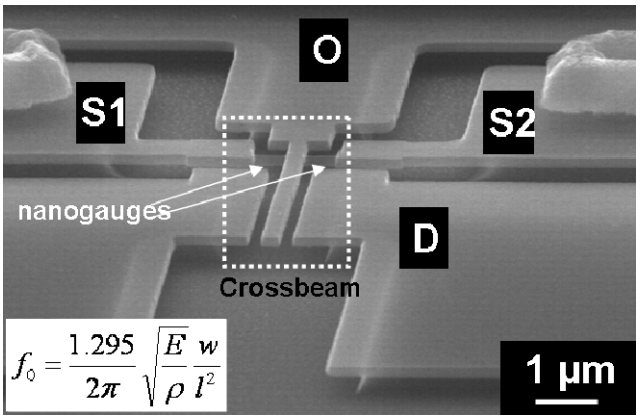

Figure 2. SEM image of a released, single-crystal silicon NEMS resonator: a so-called 'crossbeam' with its four actuation/detection ports. The bias voltages are applied on the lateral nanogauges through S1 and S2, the actuation voltages through D and the output signal V_{OUT} is measured on O. The beam dimensions are: 3.2µm long (l), 300nm wide (w), 160nm thick. The gauges width is 80nm. The inset indicates the equation of the resonance frequency f_0 of the first in-plane flexural mode (E and ρ stand for the Si Young's modulus and density).

NEMS PRINCIPLE OF OPERATION AND FABRICATION

The NEMS resonating device (Fig.2) is an electrostatically actuated (through port D), p-type, 160nm thick, silicon cantilever (3.2µm long, 300nm wide) with two lateral piezoresistive nano-gauges (400nm long, 80nm wide, ports S1 and S2) which provide an integrated electromechanical transduction of the beam mechanical motion (of the first in-plane flexural mode). Such resonators were designed for gravimetric detection of gas species. With those dimensions, these so-called 'crossbeams' (5) 43MHz resonators feature an outstanding mass sensitivity S of 17 zg/Hz (1zg=10^{-21}g). With

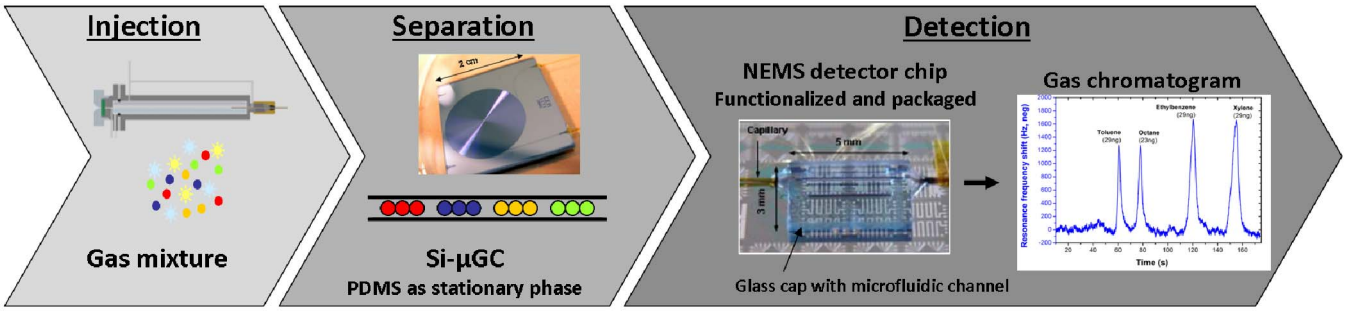

Figure 1. Schematic representation of a multi-gas analyzer associating a silicon µGC and NEMS detectors

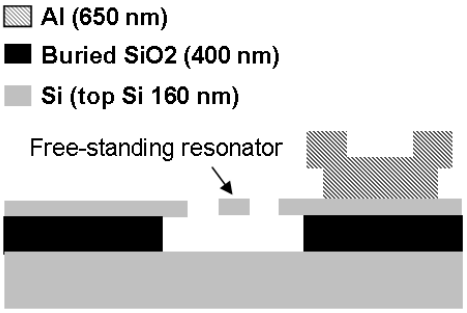

Figure 3. Simplified cross-section of the NEMS resonator and its leads (at the end of the technological process).

an experimentally measured frequency noise level around 40 Hz, it gives a mass resolution δm of 700 zg (thus a limit of detection of 2.1 ag). S and δm are given by eq.1 and 2:

$$S = \partial m / \partial f = 2m / f_0 \quad [\text{g.Hz}^{-1}] \qquad (1)$$

$$\delta m = S\,\delta f \quad [\text{g}] \qquad (2)$$

whereby m stands for the resonator mass, f_0 for the resonance frequency (see inset of Fig.2), and δf for the frequency noise, (measured through the Allan deviation $\delta f/f_0$, see below).

The fabrication process (Fig.3) is straightforward and fully compatible with CMOS front-end processes: resonators are fabricated on the 160nm thick top silicon layer of 200mm SOI wafers (with a 400nm thick buried silicon oxide). NEMS are defined by two successive deep-UV (DUV) and e-beam lithography (eBL) steps with the same resist. DUV defines all patterns except the NEMS beams and gauges which are drawn by eBL. These steps are followed by a dry etching (DRIE process) of the Si top layer. After patterning Al contacts, resonators are released by vapor-state HF acid. At the flow end, more than 97% of the 600 nanomechanical devices that were electrically tested are functional with a frequency dispersion of 1.3%.

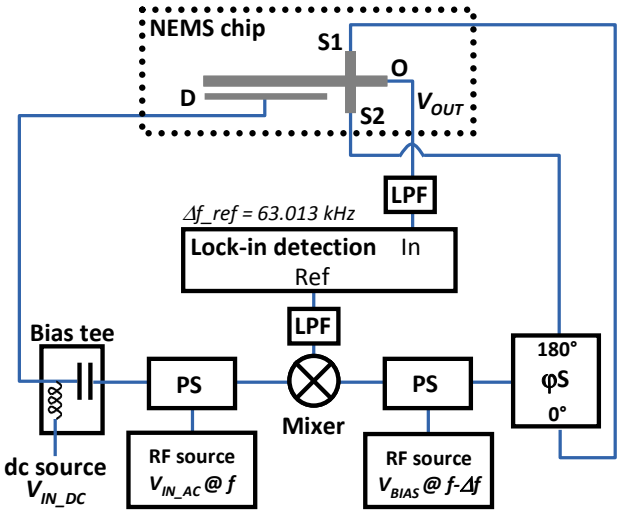

Figure 4. Heterodyne piezoresistive downmixing scheme (with one single actuation electrode) for integrated electromechanical transduction of the crossbeam mechanical motion. PS stands for power splitter, LPF for low-pass filter and φS for phase shifter.

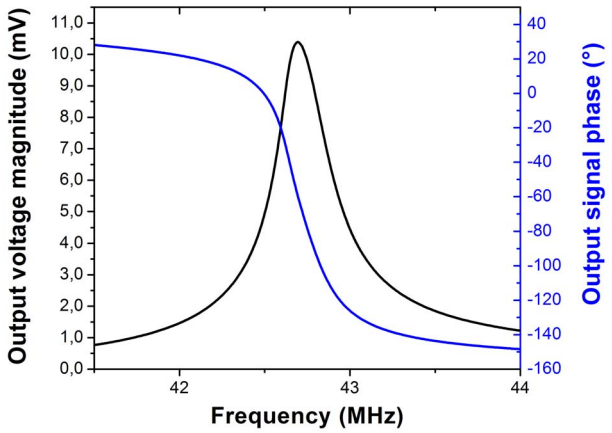

Figure 5. Open-loop frequency response measured at ambient pressure for V_{IN_AC} =2V peak-to-peak, V_{IN_DC} =10V, and V_{BIAS} =2V pp. The quality factor is 165 for a resonance frequency of 42.75MHz.

The resonator mechanical motion is detected using a heterodyne piezoresistive downmixing scheme (Fig.4) (5,6) that provides two major advantages. First, by being converted at a lower frequency (in the 10-100 kHz range), the resonance signal is below the cut-off frequency of the output low-pass RC filter resulting from the output connections (pads and cable capacitances) in series with the NEMS output resistance. Second, an excellent signal-to-background ratio is obtained (Fig.5): the feedthrough signals being at the driving and bias (high-) frequencies, they are not downconverted and are consequently filtered. At ambient pressure (as required in gas sensing applications), the output signal on resonance is larger than 10mV (without additional amplification) for a Q-factor and a resonance frequency of 165 and 42.75MHz respectively. The actuation and bias voltages, respectively V_{IN_AC}, V_{IN_DC}, and V_{BIAS} (Fig.4), were optimized so that the Allan deviation of such resonators is lower than 10^{-6} in air (Fig.6), for integration times in the range of tens of ms (required to detect fast GC elution peaks).

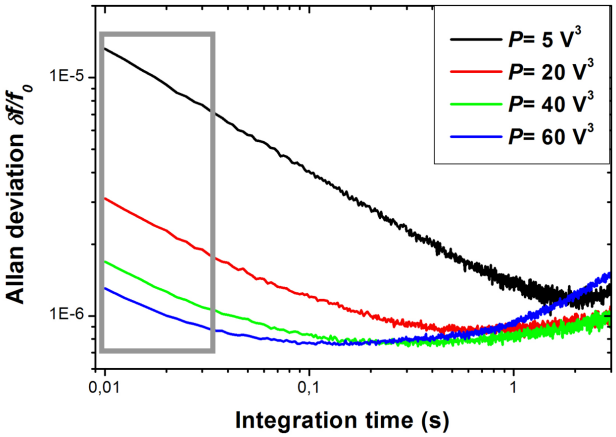

Figure 6. Allan deviation $\delta f/f_0$ of a crossbeam measured at ambient pressure for various products P=[V_{IN_AC} x V_{IN_DC} x V_{BIAS}] [V^3] (the output signal is proportional to P). In the grey region, the higher is P, the better is the resonator frequency noise as expected from [7].

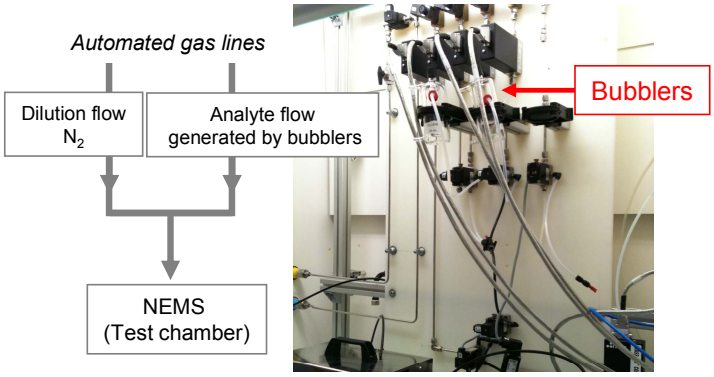

Figure 7. Gas test bench for measurements at equilibrium. Bubblers are used to generate gaseous analytes from liquid or solid origin. The concentration delivered by the bubbler as well as the flow rate, pressure, temperature and relative humidity are recorded in real time

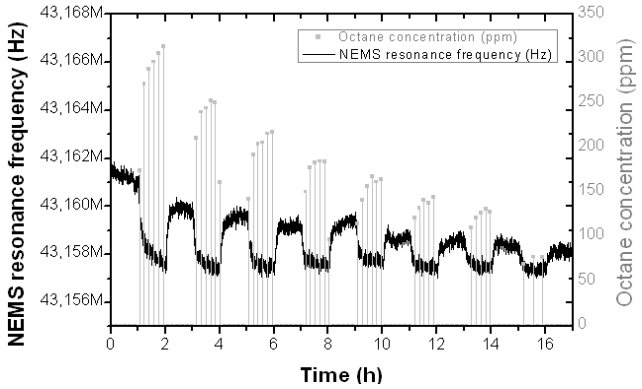

Figure 8. Gas sensing response (resonance frequency shift) at equilibrium of a blank NEMS resonator (without functionalization layer) to various concentrations of octane.

It can be shown that the NEMS output signal V_{OUT} is proportional to $V_{BIAS}(\Delta R/R)$. $\Delta R/R$ is the relative resistance variation originating from the mechanical resonance motion. These variations are dominated by the piezoresistive effect and are proportional to the applied electrostatic force, i.e. to $(V_{IN\_AC} \times V_{IN\_DC})$. As a result, V_{OUT} is proportional to the product $P = (V_{IN\_AC} \times V_{IN\_DC} \times V_{BIAS})$. It is expected from (7) that the frequency noise is theoretically given by eq.3:

$$\partial f_{MIN} = (f_0 / 2Q)\sqrt{BW / SNR} \quad \text{[Hz]} \qquad (3)$$

$$\text{with } SNR = V_{OUT}^2 / V_{NOISE}^2 \propto P^2 / V_{NOISE}^2 \quad \text{[Hz]} \qquad (4)$$

whereby V_{NOISE} is the global output noise voltage and BW the measurement bandwidth. Our Allan deviation measurements indicate that the dominant source of noise should be the readout electronics' noise. In this case, it can be expected from eq.3 and 4 that the Allan deviation is proportional to $1/P$. This is experimentally verified in the grey region of Fig.6 whereby additive white noise dominates ($1/\sqrt{f}$ slope in the Allan deviation): the higher the NEMS actuation/bias product is, the larger are the beam displacement and the related resonance signal, the better is the frequency noise. The grey region corresponds to the integration times that are required for proper operation of the gas sensor. Outside the grey region, these results indicate that for a given integration time, there is a threshold value of P for which no improvement of δf is gained. This limit is likely imposed by nonlinearities, self-heating and drift phenomena.

From a system point of view, it is required to track the resonance frequency in real-time in order to capture events of short durations (al least down to the 100ms range). In this case, an open-loop operation of the NEMS is impossible and the latter has to be operated in closed-loop. In this work, the NEMS resonator was embedded in a home-made digital phase-locked loop (8) which potentially responds faster than one ms.

GAS MEASUREMENTS

As a first step, the equilibrium response of crossbeams under various gases was measured with a dedicated test bench (Fig.7) exposing the NEMS to successive sequences of carrier gas then (analyte + carrier gas) (Fig.8). 'Blank' NEMS (without functionalization layer) and NEMS coated with a sensitive layer were exposed to different types of analytes: alkanes (Fig.9) and volatile organic compounds (VOCs). As said in the introduction, the aim is to associate a GC column to NEMS detectors: in this context, the sensor functionalization layer should not be specific to one analyte (unlike the e-nose concept) but must adsorb a large panel of gas of the same type (such as polar or non-polar molecules). Finally, we experimentally demonstrated the concept of a gas analyzer associating a silicon µGC and NEMS detectors (Fig.1). For this purpose, a miniaturized 1m long GC column (confined on a 2x2 cm^2 chip) was fabricated on a silicon wafer by DRIE, sealed with glass by anodic bonding, then internally coated with PDMS. Its input capillary was plugged behind an injector and its output was connected to

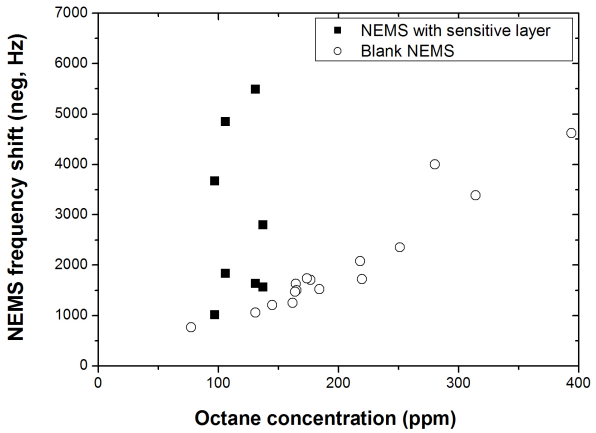

Figure 9. Example of response curves for octane: the frequency shift is plotted as a function of the concentration for several NEMS with different coating layers.

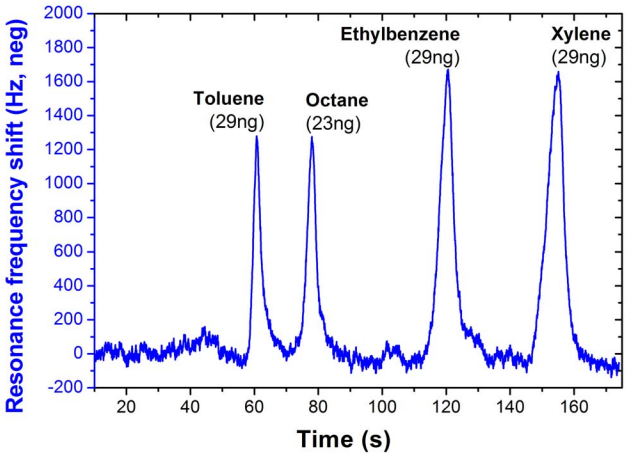

Figure 10. Chromatogram (raw data) measured by a crossbeam NEMS coated with the adsorbent layer selected after the experiments of Fig. 8 and 9. The NEMS is placed behind a miniaturized 1m long silicon µGC coated with PDMS (Fig.1), both elements are at 50°C. Brackets indicate the amount of each analyte injected into the GC column.

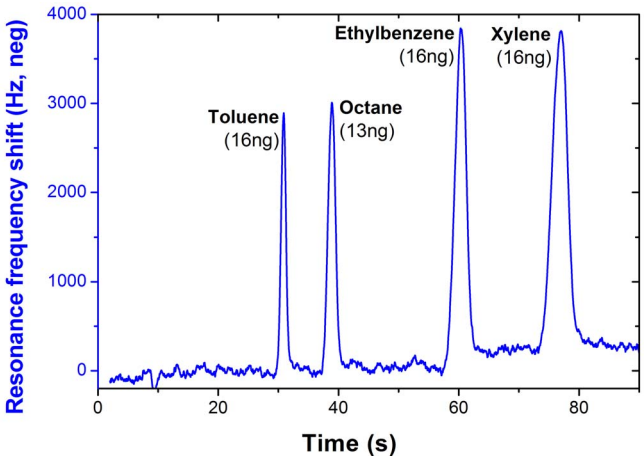

Figure 11. Chromatogram (raw data) measured by a crossbeam NEMS coated with the same adsorbent layer as in Fig.10. The NEMS (at room temperature) is placed behind a standard 2m long capillary column (at 50°C). Brackets indicate the amount of each analyte injected into the GC column. Peak maxima are larger and shorter than in Fig.10, the analysis time is divided by two.

the capillary connections of a NEMS chip. These resonators were coated with an adsorbent layer and packaged by serigraphy with a glass / polymer cap. This cap forms a confined fluidic channel above the NEMS that keeps the fluidic impedance constant with respect to the GC column. By minimizing the dead volumes at the fluidic interconnections, the loss of chromatographic resolution is very low. Fig.10 depicts a chromatogram measured by a crossbeam resonator coupled to a µGC for an injected gas mixture of four gases (one alkane and three VOCs). Fig.11 depicts another chromatogram obtained on the same mixture when coupling NEMS resonators to a 2m long standard capillary column: for each peak, the limit of detection (LOD) in terms of injected mass at the column input is below the ng level. This is at the state-of-the-art (9) when compared to a Thermal Conductivity Detector (TCD) which is the detector used in most currently existing miniaturized GC systems. In terms of perspectives, a NEMS-based analyzer could potentially contain multiple resonators that have different functionalization layers addressing different kinds of gases (such as polar or non-polar): in this case, the degree of separation of a gas mixture (4) is further increased.

CONCLUSION

The results of this work pave the way for the industrialization of ultra-miniaturized multi-gas analyzers. VLSI micro and nanofabrication techniques allow combining the well-known GC concept with ultra-sensitive gravimetric NEMS sensors.

Acknowledgements for financial support: ERC project DELPHINS, Carnot-NEMS project and CEA-NRBC program

References

(1) A.D. Wilson and M. Baietto, Sensors 9, pp.5099-5148, 2009
(2) C. Jin and E.T. Zellers, Analytical Chemistry 80, pp.7283-7293, 2008
(3) M Li, H.X. Tang and M.L. Roukes, Nature Nanotechnology 2, pp.114-120, 2007
(4) M. Li, E.B. Myers, H.X. Tang, S.J. Aldridge, H.C. McCaig, J.J. Whiting, R.J. Simonson, N.S. Lewis, and M. L. Roukes, Nanoletters 10, pp.3899-3903, 2010
(5) E. Mile, G. Jourdan, I. Bargatin, C. Marcoux, S. Labarthe, C. Kharrat, P. Andreucci, S. Hentz, E. Colinet, L. Duraffourg, Nanotechnology 21, 165504, 2010
(6) I. Bargatin, E.B Myers, J. Arlett, B. Gudlewski, M.L. Roukes, Appl. Phys. Lett. 86, 133109, 2005
(7) W. P. Robins, Phase Noise in Signal Sources, Peter Peregrinus LTD, 1982
(8) C. Kharrat, E. Colinet, A. Voda, Proc. IEEE Sensors conference, pp.1135-1138, 2008
(9) section 'Detectors in Modern Gas Chromatography' in R.L. Grob and E.F. Barry, Modern Practice of Gas Chromatography, Wiley Interscience, 2004